ECI Symposium Series, Volume RP5: Proceedings of 7th International Conference on Heat Exchanger Fouling and Cleaning - Challenges and Opportunities, Editors Hans Müller-Steinhagen, M. Reza Malayeri, and A. Paul Watkinson, Engineering Conferences International, Tomar, Portugal, July 1 - 6, 2007

CRYSTALLIZATION FOULING BEHAVIOUR OF URANIUM OXIDE AND ALUMNOSILICATE SCALE IN HIGH LEVEL NUCLEAR WASTE MEDIUM

Jonas Addai-Mensah[1], Jun Li[1] and Bill Wilmarth[2]

[1] Ian Wark Research Institute, ARC Special Research Centre.
University of South Australia. Mawson Lakes, Adelaide. 5095. SA. Australia.

[2]Westinghouse Savannah River National Laboratory
Aiken. South Carolina. USA
Corresponding author E-mail: Jonas.addai-mensah@unisa.edu.au

ABSTRACT

During high level nuclear waste (HLNW) liquor processing in evaporators operating in the temperature range 30 - 140 °C, dissolved silica, alumina, sodium hydroxide, uranium-235 and transuranic species (e.g. plutonium-238) invariably become concentrated. As the liquor evaporation proceeds, the sodium aluminosilicate (SAS) and radionuclides may exceed their solubility limits and co-precipitate, fouling the tubes and walls of the evaporator. If the fouling process is not effectively controlled or mitigated, radionuclide scale accumulation exceeding the critical mass necessary for self-sustaining nuclear fission reaction may proceed at an alarming rate, posing a serious criticality concern.

To probe the mechanisms underpinning uranium oxide-sodium aluminosilicate co-crystallization fouling, fundamental studies simulating the process were undertaken. New knowledge and greater understanding gleaned from the present work comprise crystallo-chemical structure characteristics, solubility and the fouling mechanisms involved in the mixed oxides scale deposition. The implications of the findings with regards to uranium-based scale formation in HLNW plants are highlighted.

INTRODUCTION

A serious issue that sometimes confronts HLNW processing plants in the USA is the co-deposition of sodium diuranate and aluminosilicate scale as a consequence of heterogeneous precipitation within the evaporators used in liquor concentration at the temperature range 30 - 140 °C [1-9]. The HLNW liquors are, characteristically, high ionic strength (6 - 12 M) caustic solutions mostly comprising sodium, hydroxide, silicate, aluminate, nitrite and nitrate ions and trace (< 300 $mg \cdot dm^{-3}$) radionuclides (e.g., uranium-235, plutonium-238 and caesium-137) species. As a consequence of dramatic increase in solute concentration and concomitant composition and speciation changes occurring during continuous evaporation, the liquor invariably becomes supersaturated with respect to sodium aluminosilicates and uranium (U) based species, the limiting reactants [3-6, 8-15].

The combination of high heat influx and liquor supersaturation act to facilitate the poly-condensation of solution Al(III) and SiO_2 tetrahedral species and hence, the precipitation of SAS polytypes (e.g. zeolite, sodalite and cancrinite) and occasionally sodium diuranate as scale**.** If the fissile material precipitation fouling is not effectively mitigated, scale build up, approaching 3 times the critical mass, may result and pose a serious risk [1-3,7].

Mechanistically, fouling may generally occur by a number of ways including: (i) high surface energy metal substrate-mediated heterogeneous precipitation, (ii) adsorption of existing particulate matter in suspension onto a substrate, (iii) chemical reaction solid product deposition onto an "inert" substrate, and (iv) substrate corrosion-mediated precipitation product deposition. The mechanisms and kinetics of SAS precipitation and polytypic phase transformations have been investigated under a variety of conditions [8-28]. Precipitation from highly caustic alumino-silicate media at low to moderately high supersaturations is a metal substrate (e.g., steel) - mediated heterogeneous process and may involve amorphous solid, zeolite A, sodalite and cancrinite crystals. These SAS polytypes tenaciously foul process vessel (e.g. evaporator) walls or heat exchanger tubes. The least thermodynamically stable amorphous phase is kinetically pre-disposed to form first, in contrast to the crystalline SAS phases, particularly at low temperatures (< 85 ^{o}C) [8,10,19-22, 26-28]. It rapidly transforms into zeolite A which, in turn, readily transforms into sodalite with time. Upon further crystallization, sodalite may also transform into cancrinite over several hours [10, 26, 28].

Whilst many of the reported SAS precipitation studies [9-27] have considerably advanced our understanding of aluminosilicate fouling behaviour, there is still a considerable paucity of knowledge of how the inherent polytypism specifically influences or impacts on the co-precipitation of uranium containing solute species. In previous studies [9], we showed that at low U species concentrations (< 30 $mg \cdot dm^{3}$), reflecting low relative

supersaturations ($\sigma < 2$), U species incorporation into SAS solid by adsorption is dependent upon the nature of polytype adsorbent phase(s) present. Furthermore, U species sorption loading was remarkably low, accounting for a very minor component of the overall U species that may be incorporated into SAS solids phases crystallized in HLNW liquors [9]. Thus, co-precipitation of U species with SAS is believed to be the main mechanism for the former's appearance in HLNW evaporator solids.

Given a set of solution conditions and the crystallization of various SAS solid phases, it is unclear as to how the nature and sequential evolution of the polytypes determine and/or facilitate the formation of uranium-based scale under industrially relevant conditions. In HLNW processing plants, uncontrolled fouling by radioactive solids facilitated by SAS formation may occur at an alarming rate and pose a major criticality concern, warranting complete plant shutdown for mitigation. Effective management and mitigation of both SAS and radionuclide fouling of process heat transfer equipment are, therefore, of significant importance to the HLNW industry.

In the present work, unseeded and seeded crystallization studies have been carried out to unravel the crystallo-chemical characteristics, crystallization and the concomitant fouling behaviour of uranium and sodium aluminosilicate based oxides, using simulant liquors and conditions reflecting HLNW evaporator processing.

EXPERIMENTAL

Fresh, SiO_2-free, synthetic sodium aluminate solutions were prepared from known masses of gibbsite (γ-$Al(OH)_3$) (C-31 Hydrate, Alcoa Arkansas, USA), sodium hydroxide (NaOH) (Ajax Chemicals, Australia, 97.5 % pure, 2.5 % Na_2CO_3), sodium carbonate (Na_2CO_3)(Merck, Australia, 99.9 % pure) and Milli-Q water to give a liquor of concentration 2.20-2.33 M $Al(OH)_3$, 5.4–6.0 M NaOH and 0.49 M Na_2CO_3. 0.25 dm^3 of the above liquor was placed in a 0.6 dm^3 stainless steel autoclave operating at 400 rpm agitation rate at a constant temperature. A 0.05 dm^3 solution containing 0.741 g of sodium metasilicate and 0.05 dm^3 of 6.0 M $NaNO_3$ and 6.0 M $NaNO_2$ for HLNW liquor type were sequentially added to the liquor once it had reached the required experimental temperature (30 and 65 ^oC), bringing the total liquor volume to 0.350 dm^3. To be consistent with industry solution speciation reporting norm, liquor silicon (Si) species molar concentration is expressed in terms of silica (SiO_2) whilst those of dissolved aluminium and uranium are expressed simply as Al(III) and U. A known amount of Uranyl nitrate ($UO_2(NO_3)_2$) crystals was dissolved in the final liquor to serve as a hexavalent uranium source. The final liquor compositions were: 0.01-0.1 M SiO_2, 6.6×10^{-3} -1.2 M $Al(OH)_3$, 3.8 – 6.0 M NaOH and plus either 0.38 M Na_2CO_3 for solutions ("Bayer spent liquor type") or 21 – 3400 $mg\cdot dm^{-3}$ U, 1.0 $NaNO_3$ and 1.0 $NaNO_2$ for those containing lower $Al(OH)_3$ concentration ($<6.6\times10^{-3}$ M (HLNW liquor type). Before their use, they were twice filtered through 0.45 μm membranes to give optically clear liquors.

A 316 stainless steel, high pressure Parr autoclave fitted with an external heater and an interval cooling system was used as the crystallizer for isothermal, batch precipitation runs. The vessel was fitted with a central 4 blade, 45°-pitch, 2-tier impeller which provided constant agitation at 400 rpm to within ±2 rpm. Stainless steel strips of dimensions 10 × 6 mm were attached to the shaft of the impeller to routinely provide fouled substrates for high resolution scanning electron microscopy (SEM) and powder X-ray diffraction (XRD) analysis. The control of the autoclave's temperature, heating and agitation rates were achieved through an automatic proportional, integral and derivative control system. To prevent boiling of solution above 100 ^oC, the autoclave was pre-pressurized by using H_2O vapour-saturated N_2 gas to a pressure of 3200 kPa, prior to heating. This also ensured that there was no significant solution water loss by vaporization. Continuous, plug flow precipitation experiments mimicking plant tubular heat exchanger were also conducted under other otherwise similar conditions.

Unseeded (self-nucleating) and seeded isothermal crystallization / fouling tests were run over 4 h at 30 and 65 ^oC. Solution or slurry samples were periodically removed for crystalline product characterization and solution SiO_2, Al(III) and U concentration analysis, the latter by ICP-MS (Spectro Analytical Instruments, Spectro SIM-SEQ ICP-OES, Kleve, Germany). The experimental runs were repeated 3 times for each temperature. The relative errors in SiO_2, Al(III) and U species analysis were determined to be < 3 %. Seed crystals were prepared from unseeded crystallization experiments. Particle size and its distribution were measured by laser diffraction. The specific surface area of the particles/crystals was determined by N_2 BET analysis (Coulter Omnisorp 100, Hialeah Fl. USA). Carbon coated samples were used for SEM imaging in secondary electron (SE) and backscattered electron (BSE) modes by a high resolution field emission Cam Scan (CS44FF, Cambridge, UK) at 20 or 100 kV, energy dispersive spectroscopy (EDAX). Powder XRD analysis of scale/solid product samples was also performed (Phillips PW1130/90) The XRD patterns were collected on powdered samples in $\theta/2\theta$ scanning mode using CuKα (λ = 1.5418 Å) and scan speed of 1° per min between 10° and 70° 2θ. To make BSE imaging data of fouled steel coupons more interpretable, the thick scale deposited onto the steel coupons by precipitation fouling was carefully pressed to render it flat.

RESULTS

Several secondary and backscattered electron photomicrographs of fouled steel substrates removed periodically from the crystallizer were recorded by SEM analysis. Typical, surface topographical features of the 316 stainless steel substrate used, prior to fouling, are revealed in Figure 1. Well-defined grain boundaries with variation in the size of coupon surface asperities can be clearly seen. Some of the representative images of the fouled steel coupons are shown in Figures 2 and 4. The SE images in Figures 1, 2, and 4 provide detailed morphological structures, whilst the backscattered electron (BE) images provide qualitative information on scale composition and area coverage.

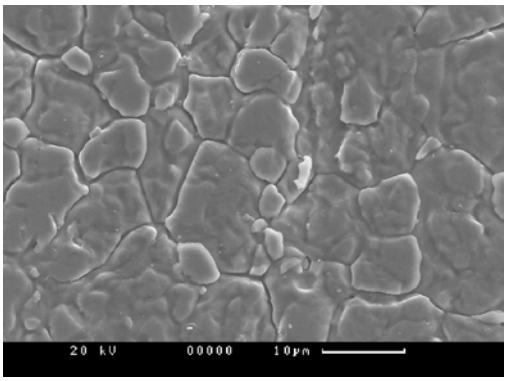

Figure 1: SEM photomicrograph of 316 stainless steel substrate before experiment.

Typical SAS solid phases crystallized from unseeded, Al(III) and SiO_2 supersaturated solution containing 0.01 M SiO_2, 0.12 M $Al(OH)_3$, 0.38 M Na_2CO_3, 1.0 M $NaNO_3$, 1.0 M NO_2 and 4.0 M NaOH are depicted in Figure 2 [10,19-22]. These images show that a scale layer of colloidal particles formed by precipitation and deposition randomly proliferate the steel substrate surface. It appears from the SEM images that the average scale particle size formed after 3 h at 30 °C was ~ 2 µm. The BSE image (B) also reveals the fractional area coverage by scale deposit whilst the high magnification SE image (C) reveals the knitted-ball particle morphology, typical of sodium aluminosilicate particles (e.g. sodalite) [10,13, 19, 21,22]. Photomicrographs obtained under similar conditions within 1 h also showed the presence of smaller but noticeable amount of scale at the steel substrate surface.

The identity of the scale as comprising sodium aluminosilicate particles from unseeded liquors at 30 and 65 °C was established by XRD analysis (Figure 3). Four distinct types of SAS phases were crystallized at different stages: initially amorphous solid and then zeolite A crystals, both of which predominated initially at lower temperatures (<65 ^{o}C), and sodalite and cancrinite crystals formed over longer periods (> 1 h) or at higher temperatures (> 65 ^{o}C). The zeolite A and its amorphous solid precursor were isostructural, exhibiting identical stoichiometric formulae: $Na_{12}Al_{12}Si_{12}O_{48}.27H_2O$. The sodalite and cancrinite crystals, on the other hand, were dimorphic and may be described as $Na_6Al_6Si_6O_{24}Na_2(NO_2^-{\cdot}NO_3^-).nH_2O$, where $2 \leq n < 4$ depending upon temperature and time.

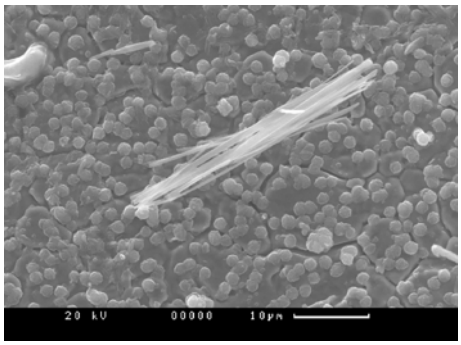

A

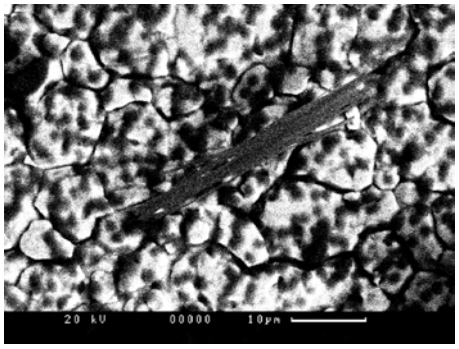

B

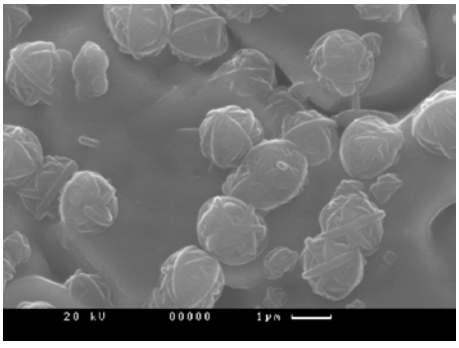

C

Figure 2: SEM low magnification SE (A) and BSE (B) and high magnification SE (C) images of fouled 316 stainless steel substrate at 3 h into experiment at 30 °C.

To crystallize a Uranium oxide phase and suppress SAS formation, an optically-clear, caustic liquor supersaturated with 3400 mg·dm^{-3} U but its Al(III) and SiO_2 concentrations at close to the equilibrium solubility of cancrinite, the least soluble SAS phase, was used. The U-compound that readily precipitated was massively aggregated, polycrystalline, platy and globular particles as revealed by the SEM SE image in Figure 4. The U-based oxide that precipitated in the temperature range 30–120 °C, without or with SAS co-precipitation, was established as sodium diuranate ($Na_2U_2O_7$) crystals by powder XRD analysis. The diffraction pattern of this oxide (Figure 5) was consistent with the international Joint Committee on Powder Diffraction's $Na_2U_2O_7$ standard reported by Kovba [29]. Furthermore, the analysis indicated that the possible presence of other iso-structural uranium oxides such as $Na(UO_2)_3O_3(OH)_2$ and $Na_6U_7O_{24}$ may be discounted [5,30].

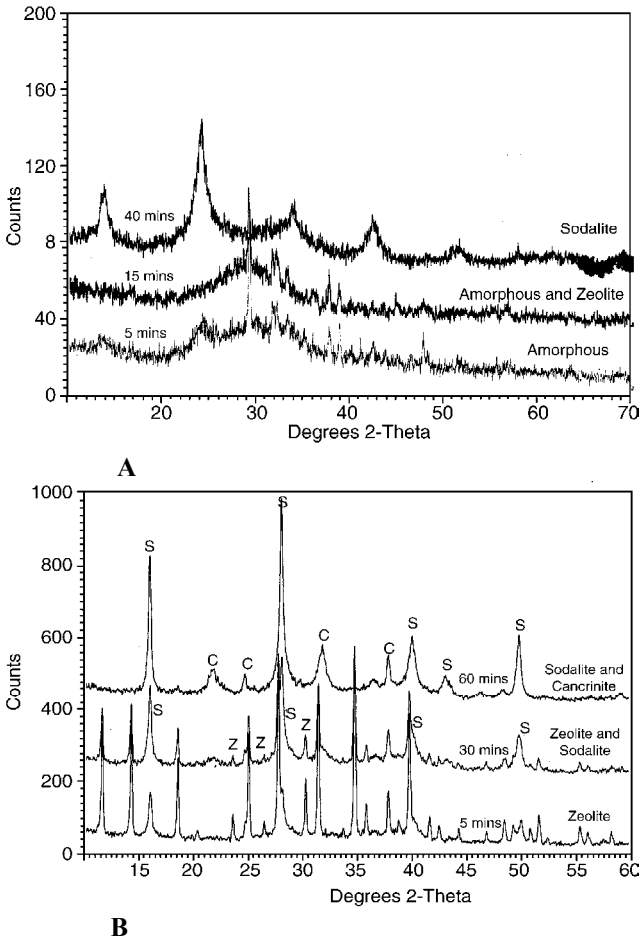

Figure 3: XRD pattern of scale formed within: 40 min at 30 °C (A) and 60 min of experiment at 65 °C (B) from an unseeded solution.

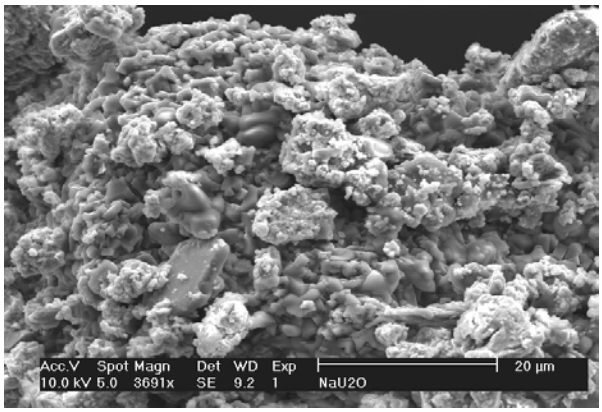

Figure 4: Typical secondary electron image of $Na_2U_2O_7$ crystals precipitated at 65 °C.

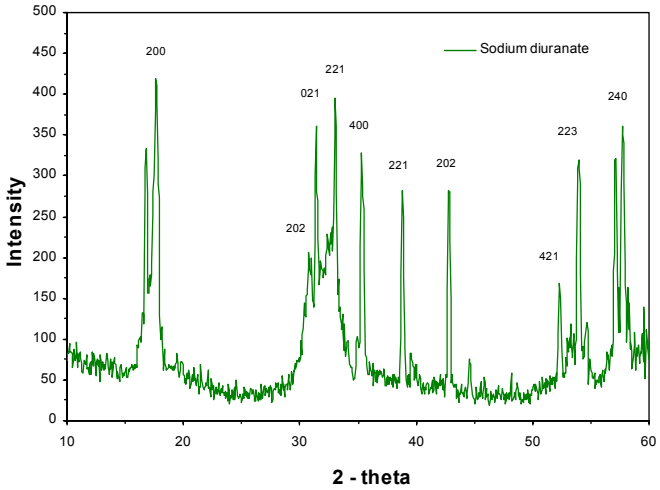

Figure 5: XRD pattern of $Na_2U_2O_7$ crystals produced by crystallization from caustic liquors at 65 °C. Diffraction peaks assignment was made in the manner of Kovba [1972].

The equilibrium solubilities of the $Na_2U_2O_7$ crystals and SAS solid phases in caustic alumino-silicate liquors of interest were determined using two types of experiments which allowed the approach to equilibrium from "above" (via seeded precipitation) and from "below" (via seeded dissolution) [11]. Under the conditions used in the present investigation, the equilibrium solubility of the $Na_2U_2O_7$ phase was in the range 9.0 – 17.0 mg·dm^{-3} U, depending upon solution composition and/or temperature. The solubilities, which agreed well with reported data [3-7 11, 30], were used in tandem with the observed instantaneous U, Al(III) and SiO_2 species concentrations to quantify the solution supersaturation with crystallization time. Typical variation of unseeded (i.e. self-nucleating) solution's U, Al(III) and SiO_2 relative supersaturations with time are shown in Figures 6. The data exemplify how rapid

desupersaturation of both SiO_2 and Al(III) species proceed at high, initial relative supersaturations ($\sigma_O > 6$) enough to induce SAS nucleation and promote U desupersaturation at low relative supersaturation ($\sigma_O = 2.4$). Following rapid desupersaturation and prolonged U-SAS mixed oxide co-precipitation, each of the three limiting reactants asymptotically approach a plateau value within 2 h.

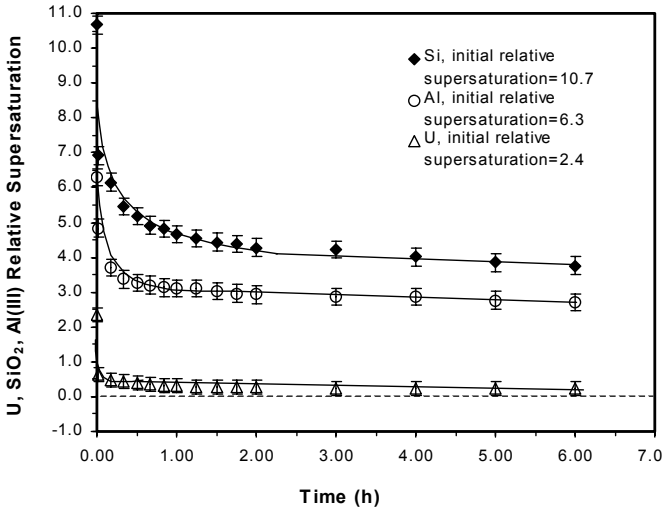

Figure 6: U, SiO_2 and Al(III) relative supersaturation as a function of time during crystallization of U-based oxide SAS with at 30 ^oC (initial solution: NaOH = 4.0 M, $NaNO_3$ = 1.0 M, $NaNO_2$ = 1.0 M, SiO_2(♦)= 175.0 × 10^{-3} M, Al(III) (○) = 175.0 ×10^{-3} M and U (Δ)= 30.8 mg·dm^3.

The scale deposits which precipitated from the U, SiO_2 and Al(III) supersaturated liquors were established to be mixed sodium diuranate and aluminosilicate (e.g., amorphous solid, zeolite, sodalite) phases by powder XRD, backscattered electron image and energy dispersive spectroscopy analyses. Fouling occurring as a result of U-SAS mixed oxides' heterogeneous nucleation and growth mechanisms at moderate to high U supersaturations characteristically resulted in the formation of both discreet and middling particles of $Na_2U_2O_7$ and SAS phases.

Representative SEM BSE image and EDAX data obtained for a U-SAS mixed oxide fouled steel coupon are displayed in Figure 7. For the mixed phase scale, the BSE analysis provides atomic number-defined, phase-specific structural information whilst the EDAX data reveal elemental Al, O, Si, U and Na compositions of the selected areas. The white and dark regions in Figure 7 (A) represent U and SAS oxide rich regions, respectively, as established by the corresponding EDAX analysis (Figure 7(B and C)). The crystallographic characteristics of the two oxides were confirmed by complementary powder XRD analysis.

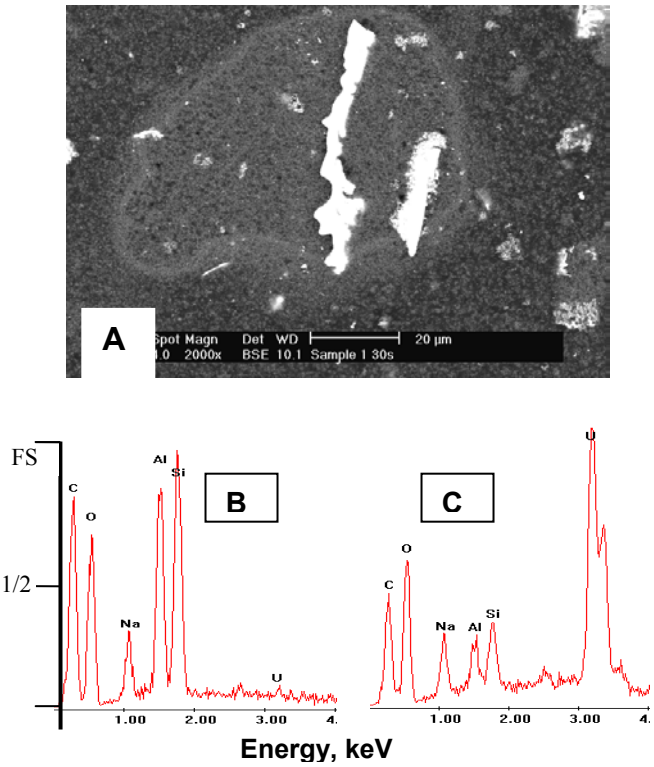

Figure 7: SEM BSE image (A) of fouled steel substrates due to co-precipitation of SAS (dark area) and sodium diuranate (white areas) at 65 ^oC; EDAX analysis of SAS-rich region (B) (in dark area in A) and sodium diuranate-rich region (C) (in white areas in A). The carbon (C) signal is due to the background.

DISCUSSION

At a given initial SiO_2 and Al(III) supersaturation, the rate of isothermal precipitation of the ephemeral amorphous SAS was found to be the highest and that of cancrinite the lowest, consistent with the thermodynamic stabilities of these phases and in agreement with the lowest and greatest activation barriers involve for nucleation and growth, respectively, for the former and the latter. As a consequence of heterogeneous nucleation and growth of SAS solid phases, which impacted on U species precipitation, the overall U and SiO_2 or Al(III) desupersaturation rate per equivalent SAS particle surface area followed the sequence:

Amorphous > Zeolite A > Sodalite > Cancrinite **(1)**

Routine analytical techniques (SEM imaging, EDAX and XRD analyses) were used as valuable, complementary tools in the mixed U-SAS oxide scale phases' identification. The secondary electron imaging revealed details of steel substrate and scale deposit structural information in terms of

particle morphology and size, whilst the backscattered electron imaging and EDAX provided vital contrast information on different crystallo-chemical structures present in the multi-phase solid scale or the compounds in the scale composite [31]. For the flat, massive SAS-U oxide scale deposit prepared and analyzed in the present work (e.g., as in Fig. 7(A)), the SEM electron backscattering uniquely depends on the average atomic number of the target solid sample (i.e. scale). In a BSE image of such a flat multiphase scale sample, regions of high and low signals correspond to the highest and lowest atomic numbers, respectively. These signals characteristically translate into two distinct regions of colour where the highest atomic number (i.e. U in this case) appeared as white, whilst that of the lowest (i.e. Al and Si) appeared as dark area, as recourse to Figure 7(A) and EDAX bulk elemental Al, O, Si, U and Na composition analysis (Fig. 7(B and C)) shows.

Furthermore, the dissipation of U species supersaturation was fairly rapid initially and dependent upon the type of the dominant SAS phase(s) crystallizing. Initial liquor U concentrations in the range 70 – 3400 $mg{\cdot}dm^3$ may be readily reduced to ≈ 13 $mg{\cdot}dm^3$ after 6 h by a strong, SAS-mediated heterogeneous nucleation and growth at a total solid surface area of 260-270 $m^2{\cdot}dm^{-3}$ liquor. The SAS mediation of U precipitation was greater when both nucleation and growth (of SAS) mechanisms prevailed than just the latter. At high very U relative supersaturation (σ_u >300), sodium diuranate precipitation was observed to be substantially independent of the rate of SAS co-precipitation. On the other hand, U desupersaturation rate was negligibly small at relative supersaturations (σ_u) < 2 or U species concentration < 30 $mg{\cdot}dm^{-3}$ and SAS supersaturation is close to zero. Thus, in the absence of SAS precipitation (i.e. under SAS equilibrium solubility conditions) and at low U supersaturation $Na_2U_2O_7$ appreciable crystallization, U ions adsorption onto SAS solids may become important. It is pertinent to note, however that, the extent of U adsorption is strongly dependent upon the SAS polytype type and solid mass loading, especially for Mesoporous amorphous solid and zeolite A phases [8]. These findings indicate that SAS heterogeneous nucleation and growth is a critically important mediation process for U oxide co-precipitation at low to moderate solution supersaturations in HLNW evaporators. Further investigation and characterization of the mixed sodium diuranate and sodium aluminosilicate precipitation fouling kinetics will be useful for prediction of the evolution of mixed oxide scale layer nucleation and growth.

CONCLUSIONS

The information gleaned from several isothermal crystallization and scale characterization studies of sodium aluminosilicate and sodium diuranate at 30 and 65 ˚C reveal new and important crystallo-chemical information and a mechanistic basis of uranium-enriched SAS scale formation.

1. The rate of SAS and mixed SAS-U oxide crystallization from seeded solutions followed the order: Amorphous > Zeolite A > Sodalite > Cancrinite.
2. The uranium-solid phase that crystallized from highly caustic, sodium aluminosilicate saturated or supersaturated liquors was sodium diuranate oxide phase.
3. Sodium diuranate co-precipitated as both discreet and middling particles with amorphous/gel and crystalline SAS polytypes (zeolite A, sodalite and cancrinite) at moderate to high U supersaturations.
4. SAS phase co-precipitation via nucleation and growth is necessary for the mediation of heterogeneous precipitation of sodium diuranate from liquors at low to moderate U supersaturations.

ACKNOWLEDGEMENT

The financial support provided by Westinghouse Savannah River Company (Aiken, USA) for this research project is gratefully acknowledged.

REFERENCES

1. Wilmarth, W.R. Thompson, M.C., Martino, C.J. Dukes, J.T., Boley, C.S. and Lewis, B.L. (2003). Nitric acid cleaning of a sodalite-sodium diuranate scale in high level waste evaporators, Separation Science and Technology 38 12/13 3249.
2. Oji L.N. and Williams, A. (2002). Incorporation of Uranium into sodium aluminosilicate Phase. US Department of Energy -WSRST Report No. SRT-LWP-2002-00109.
3. Hobbs, D. T. and Edwards, T. B. (1994). Solubility of uranium in alkaline salt solutions. US Department of Energy-WSRC Report TR-93-454.
4. Cordfunke, E. G. P and Loopstra, B. O. (1971). Sodium Uranates: Preparation and Thermochemical *Properties*, J. Inorg. Nucl. Chem. 33 2427-2436.
5. Giammar, D. E. and Hering, J. G. (2002). Equilibrium and kinetic aspects of soddyite dissolution and secondary phase precipitation in aqueous suspension, Geochim. Cosmochim. Acta, 66, 18, 3235-3245.
6. Puigdomenech, I. and Bruno, J. (1988). Modeling uranium solubilities in aqueous solutions: validation of a thermodynamic database for the EQ 3/6 Geochemical Codes, Swed. SKB Tech. Rep., SKB 88-21.
7. Duff, M. C. (2002). Uranium interactions with sodium aluminosilicates: Part 1 Sorption. US

Department of Energy-WSRS Report No. SRT-LWP-2002-00109.
8. Addai-Mensah, J. Li, J. and Zbik, M. (2002). Sodium aluminosilicate solid phases: Chemistry and crystallization behaviour. WSRS/ERDA Report No. G008.
9. Addai-Mensah, J., Li, J., Zbik, M. and Wilmarth, W.R. (2005). Uranium sorption in sodium aluminosilicate phases under caustic conditions. Separation Science and Technology 40 267.
10. Addai-Mensah, J., Li, J., Zbik, M. and Rosencrance, S. (2004). Sodium aluminosilicate solid phase specific fouling behaviour. Int. J. of Transport Phenomena 6 111.
11. Addai-Mensah, J. Li, J., Rosencrance, S., Wilmarth, W. R. (2004). Solubility of amorphous sodium aluminosilicate and zeolite A solid phases in nitrate/nitrite-rich caustic aluminate liquors. J. Chemical and Engineering Data 204 171.
12. Barnes, M. C., Addai-Mensah, J. Gerson A. R. and Smart, R. St.C. (1999). The solubility of sodalite and cancrinite in synthetic spent Bayer liquor. Colloids and Surfaces A 157 (1-3) 101.
13. Zheng, K. Gerson, A.R. Addai-Mensah J. and Smart, R. St.C. (1997). The influence of sodium carbonate on aluminosilicate crystallization and solubility in sodium aluminate solutions, J. Crystal Growth 171, 197.
14. Zheng, K. Smart, R. St.C. Addai-Mensah, J. and Gerson, A.R. (1998). Solubility of sodium aluminosilicates in synthetic Bayer liquor. J. Chemical and Engineering Data 43 3 312.
15. Breuer, R.G. Barsotti L.R. and Kelly, A.C. (1963). Behaviour of silica in sodium aluminate solutions', Extractive Metallurgy of Aluminium Vol. 1. Alumina, Interscience, New York, 133.
16. Roach, G.I.D, and Cornell, J.B. (1985). Scaling in Bayer plants. Proceedings of Australian Chemical Engineering Annual conference, Chemeca 85, Paper B7A 217.
17. Ostap, S. (1985). Control of silica in the Bayer process used for alumina production, Impurity control Disposal, Proc., CIM Annual Hydrometallurgy Meeting, 15th 14.
18. O'Neill, G.A. (1986). Prediction of heat exchanger-heat transfer co-efficient decay due to fouling. Light Metals 133.
19. Addai-Mensah, J., Gerson, A.R. Jones, R. and Zbik, M. (2001). Reduction of Sodium Aluminosilicate scale in Bayer plant heat exchangers. Light Metals 13.
20. Addai-Mensah, J., Barnes, M.C. and Gerson, A.R. Fouling of alumina refining heat exchangers: Effect of substrate and temperature. Proceedings 6th World Congress of Chemical Engineering, Melbourne Australia (2001) 1.
21. Addai-Mensah, J., Gerson A.R. and Smart, R. St. C. (1998). Continuous plug flow precipitation of sodalite scale on steel heat transfer surfaces. Light Metals 21.
22. Addai-Mensah, J. Gerson, A.R., Zheng, K O'Dea, A. and Smart, R.St.C. (1997). The precipitation mechanism of sodium aluminosilicate scale in Bayer plants. Light Metals, 23.
23. Barnes, M.C. Addai-Mensah J. and Gerson, A.R. (1999). The kinetics of desilication of synthetic spent Bayer liquor seeded with cancrinite and cancrinite/sodalite mixed-phase crystals. J. Crystal Growth 200, 251.
24. Barnes, M.C., Addai-Mensah, J. and Gerson, A.R. (1999). The kinetics of desilication of synthetic spent Bayer liquor seeded with pure sodalite, pure cancrinite and their dimorphic mixed phase crystals. Light Metals 121.
25. Barnes, M.C., Addai-Mensah, J. and Gerson, A.R. (1999). The kinetics of desilication of synthetic spent Bayer liquor and sodalite crystal growth. Colloids and Surfaces A 147, 283.
26. Barnes, M.C., Addai-Mensah J. and Gerson, A.R. (1999). The mechanism of the sodalite-to-cancrinite phase transformation in synthetic spent Bayer liquors. J. Microporous and Mesoporous Materials 31, 287.
27. Barnes, M.C., Addai-Mensah, J. and Gerson, A.R. (1999). A methodology for quantifying sodalite and cancrinite phase mixtures and the kinetics of the sodalite to cancrinite phase transformation. Mesoporous and Macroporous Solids 31 303.
28. Gerson, A.R., Addai-Mensah, J., Zheng, K., O'Dea, A. and Smart, R.St.C. (1996). The mechanism of sodium aluminosilicate scale formation in Bayer refineries. Proceedings of the 4th International Alumina Quality Workshop, Darwin, Australia, 393.
29. Kovba, L. M. (1972). Crystal structure of sodium diuranate, Radiokhimiya 14, 5, 727.
30. Chernorukov, N. G. and Kortikov, V. E. (2001). $Na[HSiUO_6]$ H_2O: Synthesis, Structure and Properties. Radiochem. 43, (3) 229.
31. Surface Analysis Methods in Materials Science, O'Connor, D.J., Sexton, B.A. and Smart, R. St.C. (Eds), 2nd. Ed., Springer Pub. Berlin/New York/London, (2003).